2328-21

Preparatory School to the Winter College on Optics and the Winter College on Optics: Advances in Nano-Optics and Plasmonics

30 January - 17 February, 2012
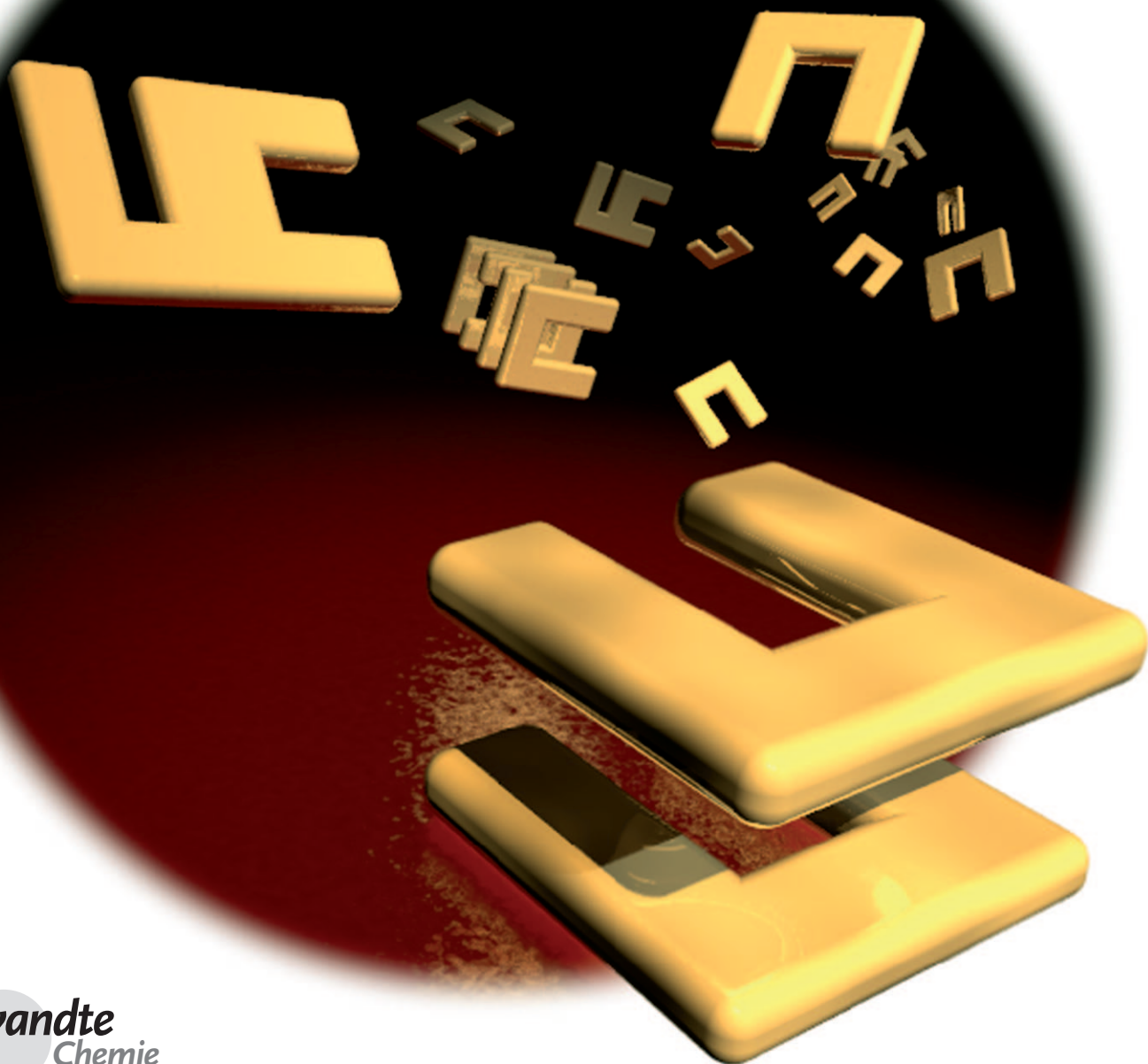
Coupling Effects in Optical Metamaterials

H. Giessen

Physikalisches Institut
Stuttgart
Germany

Metamaterials

Coupling Effects in Optical Metamaterials

Na Liu and Harald Giessen*

*M*etamaterials have become one of the hottest fields of photonics since the pioneering work of John Pendry on negative refractive index, invisibility cloaking, and perfect lensing. Three-dimensional meta-materials are required for practical applications. In these materials, coupling effects between individual constituents play a dominant role for the optical and electronic properties. Metamaterials can show both electric and magnetic responses at optical frequencies. Thus, electric as well as magnetic dipolar and higher-order multipolar coupling is the essential mechanism. Depending on the structural composition, both longitudinal and transverse coupling occur. The intricate interplay between different coupling effects in a plasmon hybridization picture provides a useful tool to intuitively understand the evolution from molecule-like states to solid-state-like bands.

From the Contents

1. Introduction

Metamaterials are artificial materials with designed electromagnetic functionality and sizes much smaller than the operating wavelength of light.[1–4] Metamaterials often consist of metallic nanostructures, which allow the possibility to tailor their optical properties. Incident light can excite coherent oscillations of free conduction electrons, which leads to localized particle plasmon resonances.[5,6] The resonance frequencies depend on the size, shape, and dielectric function of the metal, as well as the dielectric function of the surrounding environment.[7,8] The shape of the individual metamaterial constituents can vary substantially: from simple spheres or ellipsoids to wires,[9,10] split-ring resonators (SRRs),[11,12] meshes,[13,14] to meanders.[15,16] Metamaterials can offer new properties that natural materials do not have. For example, a negative magnetic permeability can be engineered.[9–12,17] This property together with their negative electric permittivity[18] can lead to metamaterials that exhibit a negative refractive index.[19–23] These astounding properties are well suited for novel devices such as superlenses[24,25] and hyperlenses[26] which surpass the diffraction limit, or optical cloaks that can render objects invisible.[27–29]

For practical applications of metamaterials, three-dimensional or even bulk structures are often needed. Since the size of the metamaterial constituents and hence the unit cells are much smaller than the wavelength of light, the lateral as well as vertical finite spacing will inherently lead to strong interaction between the neighboring metamaterial elements.[30–33] As a result, the optical properties can be changed substantially compared to those of an individual metamaterial element.[32,33] This is analogous to solid-state physics, where the electronic properties of solids can vary dramatically from those of individual atoms; take for example carbon, where the optical spectra of individual atoms differ strongly from those of graphite or diamond.[34] This example also illustrates that the arrangement of the unit cells in the lattice of the solid is crucial for the resulting properties.

We have divided our Review on coupling effects in optical metamaterials into several parts. First, we show the funda-mental principles of dipole–dipole interactions in the electro-static regime.[35] Then we start from very simple plasmonic structures, such as gold nanowires, and briefly discuss their resonant behavior. We will then consider dimers of gold nanowires that can be coupled together transversely as well as longitudinally. We will further show that this design can act as an artificial magnetic "atom".[17] Subsequently, we will introduce another artificial magnetic "atom", the split-ring resonator, which allows an extra degree of freedom—namely the inclusion of a magnetic response—in the coupling.[11,12] In fact, when split-ring resonators are coupled one needs to consider the magnetic interaction in addition to the electric interaction.[36–39] Subsequently, we will show coupled split-ring resonators of different complexity. Finally, we will highlight several three-dimensional metamaterials based on different stacked structures and discuss their coupling effects in detail.[40–42] We believe that an understanding of the funda-mental coupling mechanisms will provide significant insight into the design and optimization of metamaterial structures with desirable optical properties as well as resonant behavior.

[*] Prof. Dr. H. Giessen
4. Physikalisches Institut and Research Center SCOPE
Universitaet Stuttgart
Pfaffenwaldring 57, 70569 Stuttgart (Germany)
Fax: (+49) 711-685-65097
E-mail: giessen@physik.uni-stuttgart.de
Homepage: http://www.pi4.uniso-stuttgart.de/NeueSeite/
index.html

Dr. N. Liu
Materials Science Division
Lawrence Berkeley National Laboratory
Berkeley, CA 94720 (USA)

2. Theoretical Basics of Dipole–Dipole Coupling

It is quite straightforward to derive the interaction energy when coupling two dipoles together, either electric or magnetic ones, from a simple quasistatic picture.[35] For simple geometries it is sufficient to consider longitudinal or transverse interaction. Here we will limit ourselves to a first approximation to only the dipole–dipole interaction, although higher-order multipoles can play a substantial role in metamaterials.[38,43,44]

As shown in Figure 1, if two dipoles with dipole moments $\vec{p}_1$ and $\vec{p}_2$ (either electric or magnetic) interact at center-to-
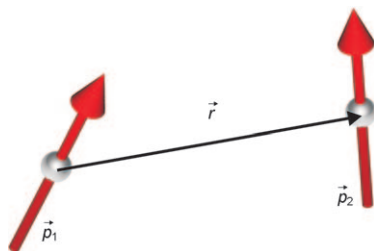
Figure 1. The interaction between two dipoles $\vec{p}_1$ and $\vec{p}_2$ with $\vec{r}$ being the center-to-center vector.

center distance r, the quasistatic interaction energy V is given by Equation (1). This relationship reduces to Equation (2) for purely transverse (side-by-side alignment) or longitudinal (end-to-end alignment) coupling of the two dipoles.

$$V = \frac{1}{4\pi\varepsilon_0}\left(\frac{\vec{p}_1\cdot\vec{p}_2}{r^3} - \frac{3(\vec{p}_1\cdot\vec{r})(\vec{p}_2\cdot\vec{r})}{r^5}\right)$$
$$= \frac{\vec{p}_1\cdot\vec{p}_2 - 3(\vec{p}_1\cdot\hat{r})(\vec{p}_2\cdot\hat{r})}{4\pi\varepsilon_0 r^3} \tag{1}$$

$$V = \gamma\frac{p_1\cdot p_2}{4\pi\varepsilon_0 r^3} \tag{2}$$

with $\hat{r}$ as the unit vector from $\vec{p}_1$ and $\vec{p}_2$. γ is the interaction index, which is $+1$ for transverse coupling and -2 for longitudinal coupling. p_1 and p_2 are the magnitudes of the dipole moments.
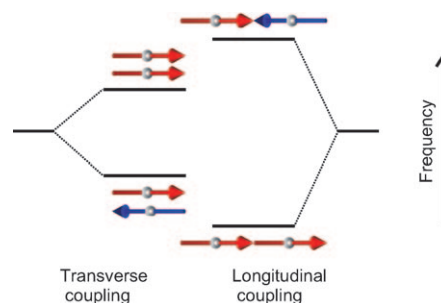
Figure 2. Level scheme of two coupled dipoles. Left: Transverse coupling. Right: Longitudinal coupling. The vertical axis corresponds to the resonance frequency.

Figure 2 shows the level scheme of two coupled dipoles for both transverse and longitudinal coupling. In the case of transverse coupling (for example, two electric dipoles), laterally coupled dipoles in the antisymmetric mode attract each other, hence decreasing the restoring force and leading to a lowering of the resonance frequency. In contrast, two symmetrically ordered dipoles are repulsive, and hence give rise to an enhanced restoring force that leads to a higher resonance frequency. The opposite holds true for longitudinally coupled dipoles: there, a symmetric arrangement leads to an attraction of the opposite charges and therefore decreases the restoring force and leads to a lowering of the resonance frequency. The high-frequency mode, on the other hand, is represented by the antisymmetric arrangement of the two dipoles, in which the restoring force is increased due to the repulsion of charges with the same sign. Similarly, for transverse (longitudinal) coupling of two magnetic dipoles, the repulsion and attraction of the two north and south poles will lead to an enhanced (reduced) magnetic interaction and therefore a higher (lower) resonance frequency.

3. Artificial Metamaterial "Atoms"

### 3.1. Single Metallic Nanoparticles

Let us start with the optical properties of a single metallic nanoparticle, for example, a gold nanowire with a size of $500\times150\times20$ nm^3. It resides on a glass substrate and is illuminated

Na Liu was born in Shenyang (China). She received her BSc in Physics from Jilin University (China) in 2001 and completed her MSc in Physics at the Hongkong University of Science and Technology in 2005. She obtained her PhD in the 4th Physics Institute at the University of Stuttgart (Germany) in 2009. Her research interests include the design, fabrication, and characterization of three-dimensional optical metamaterials. Since 2010, she has been carrying out postdoctoral research at the Materials Science Division, Lawrence Berkeley National Laboratory, USA.

Harald Giessen is the director of the 4th Physics Institute at the University of Stuttgart. He obtained his diploma in Physics at the University of Kaiserslautern in 1992, and his MSc and PhD as a J. W. Fulbright scholar from the Optical Sciences Center at the University of Arizona in 1994 and 1995, respectively. After postdoctoral research at the MPI (Stuttgart) and the University of Marburg, 2001–2004 he was Associate Professor at the University of Bonn. Since 2005 he has been Full Professor at the University of Stuttgart. His interests are ultrafast nano-optics, particularly metamaterials and plasmonics as well as white-light lasers.
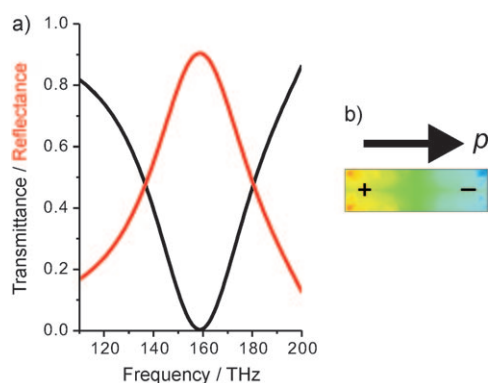
Figure 3. a) Simulated transmittance and reflectance spectra of a gold nanowire structure. The normally incident light is polarized along the longer axis of the nanowire. b) The electric field distribution at the resonance. Positive (red) and negative (blue) charges are excited at the ends of the nanowire. This corresponds to the excitation of an electric dipole moment.

Figure 4. Transverse coupling of two coupled metallic nanowires. A magnetic dipole moment can be excited in the antisymmetric mode and acts as a magnetic "atom".
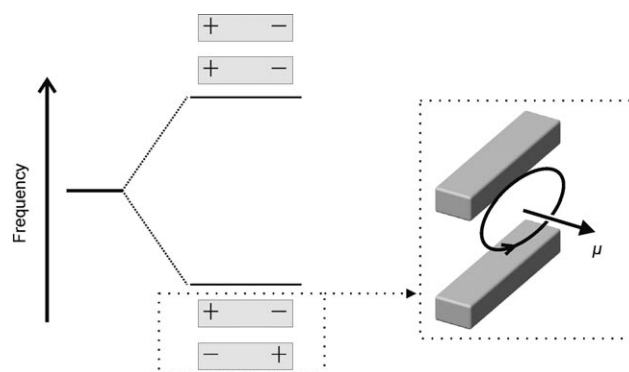
by light which is linearly polarized along the longer axis of the nanowire at normal incidence. As shown in Figure 3a, a resonance can be observed at around 160 THz (ca. 1870 nm or 5340 cm^{-1}) in the spectrum. Associated with this resonance is the excitation of an electric dipole moment in the nanowire which extends from the negative to the positive charges (see Figure 3b).[5–7] All the simulated spectra and field calculations in this Review were performed by using the software package CST Microwave Studio.

3.2. Coupled Metallic Nanowire Pairs as Magnetic "Atoms"

We further consider two gold nanowires with a finite separation.[9,10,17,45–47] The two nanowires are strongly coupled because of the proximity. The interaction can lift the bare plasmonic mode of the individual nanowires and leads to two new modes as a consequence of plasmon hybridization:[48–52] one with a symmetric alignment of the two electric dipoles and one with an antisymmetric alignment. This plasmon hybridization picture, which was introduced by Peter Nordlander, demonstrates a compelling analogy between plasmon resonances of metallic nanoparticles and wavefunctions of simple atoms and molecules.[48–52] The assignment as to which alignment represents the lower-frequency resonance and which one represents the higher-frequency resonance depends crucially on how the two nanowires are arranged with respect to one another, as discussed in Section 2.[40,53–55]

In particular, the antisymmetric mode of the two nanowires in the transverse configuration is also termed "magnetic resonance".[17,45–47] The reason for this terminology is as follows: the antisymmetric currents in the two wires together with the displacement currents between the two wires can lead to a resonant excitation of the magnetic dipole moment (Figure 4), thereby giving rise to a magnetic response in the system.

Therefore, two nanowires in a stacked fashion can act as a magnetic "atom", which is one of the fundamental building block of metamaterials. As we will show later, one can construct stacked metamaterials by combining several layers of these "atoms" together and taking their coupling into account.[40]

3.3. Metallic Split-Ring Resonators as Magnetic "Atoms"

The split-ring resonator (SRR) structure is another fundamental building block of metamaterials.[11,12] It has been widely utilized for constructing materials with negative permeability or even negative refractive index when combined with materials that contain continuous wires.[19–23] When linearly polarized light is incident along the gap-bearing side of an SRR at normal incidence,[56] electric dipole-like plasmons can be excited in the entire SRR, thus giving rise to a magnetic dipole moment perpendicular to the SRR plane (Figure 5). When two such split-ring "atoms" are arranged in different configurations, for example, next to each other or
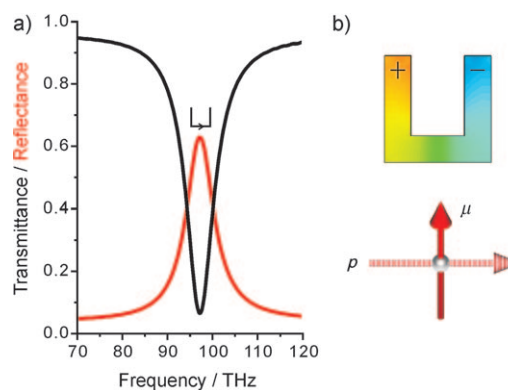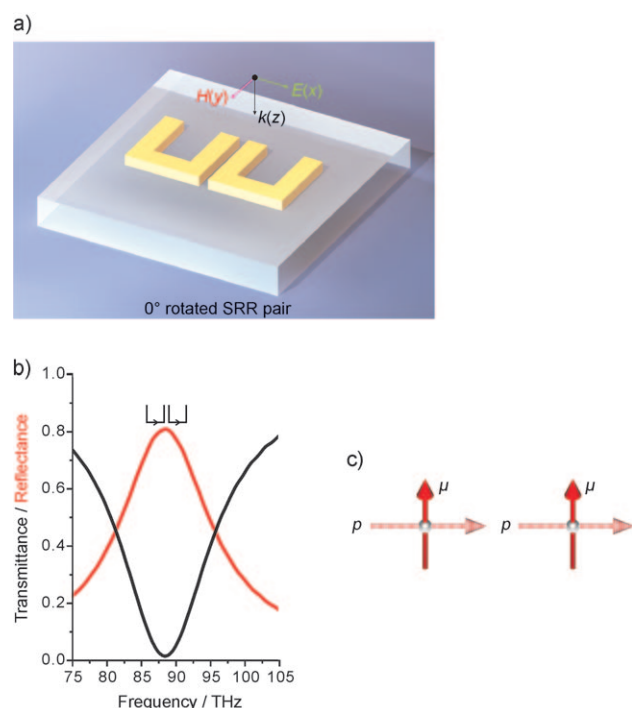

Figure 5. a) Simulated transmittance and reflectance spectra of a gold split-ring structure on a glass substrate. The size of the split ring is 400×400 nm^2. The arm width is 100 nm and the gold thickness is 50 nm. The normally incident light is polarized along the gap-bearing side of the split ring. The symbol represents the currents in the split ring at the resonance. b) The electric field distribution at the resonance. Electric dipole-like plasmons are excited along the entire split ring, thereby giving rise to a magnetic dipole moment perpendicular to the split-ring plane. The solid and dashed arrows represent magnetic and electric dipole moments, respectively.

above each other, similar coupling rules as in the case of the electric dipoles apply to the magnetic dipoles. However, the coupling behavior is more complex than the case of two coupled metallic nanoparticles because of the fact that both the electric as well as the magnetic coupling should be taken into account. Also, it is not clear which coupling mechanism is dominant. As we will show later, it is possible to reduce or even switch off the electric dipolar coupling and retain only the magnetic coupling,[36,38,42] which in turn simplifies the understanding of the coupling mechanisms of rather complex metamaterial systems.

4. Lateral Coupling of Split-Ring Resonators

In this section we investigate planar split-ring dimers, which consist of laterally coupled split-ring pairs with a certain rotation angle.[36] Let us first consider a side-by-side configuration with a 0° rotation angle between the two split rings (Figure 6a). The polarization of the normally incident light is along the gap-bearing side of the split rings. In this case, the light excites circulating currents in the split rings which correspond to the excitation of two electric dipoles oriented along the direction of the gaps in the split rings. The
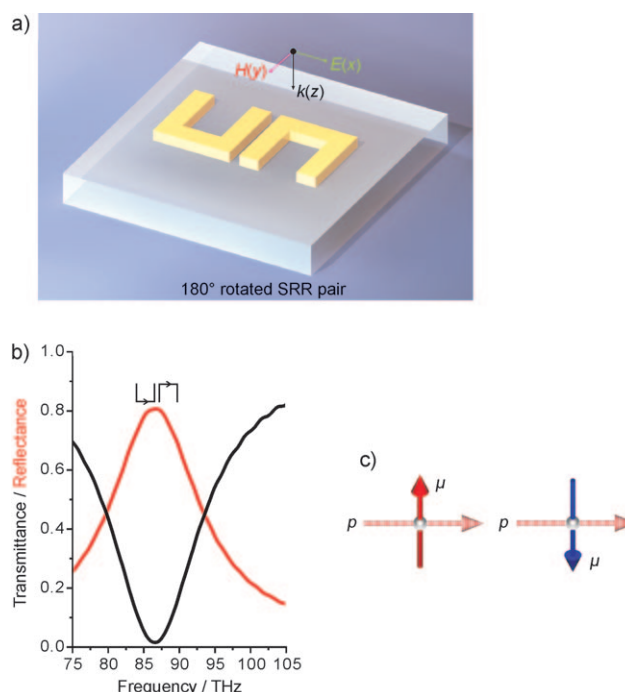
two resulting magnetic dipoles are perpendicular to the plane of the split rings. As a result, the two electric dipoles are longitudinally coupled whereas the two magnetic dipoles are transversely coupled. As there is no phase retardation between the two split rings (because of the normal incident light), they are excited symmetrically. Hence, the spectrum of the 0°-rotated split-ring pair shows only a single resonance (Figure 6b). At the resonance frequency the two electric dipoles are aligned parallel, as are the two magnetic dipoles (Figure 6c). Tilted incident light would cause symmetry breaking and introduce a certain lateral phase shift between the two split rings, thus making the antisymmetric mode weakly observable.[57]

Similarly, for the 180°-rotated split-ring pair depicted in Figure 7a, only a single resonance can be observed in the spectrum because of the lack of phase retardation (Figure 7b). At the resonance frequency the two electric dipoles are aligned parallel, whereas the magnetic dipoles are aligned antiparallel because of the 180° rotation of the split ring on the right (Figure 7c).

The situation becomes intriguing for the 90°-rotated split-ring pair,[36,58] as shown in Figure 8a. Circulating currents in the right split ring cannot be directly excited by the external light because of its orientation with respect to the incident

Figure 6. a) Schematic representation of the 0°-rotated split-ring pair on a glass substrate. The size of each split ring is 400×400 nm². The arm width is 100 nm and the gold thickness is 50 nm. The separation between the two split rings is 50 nm. The normally incident light is polarized along the *x* direction. b) Simulated transmittance and reflectance spectra of the 0°-rotated split-ring pair. The symbols represent the currents in the split rings at the resonance frequency. c) Schematic diagram of the alignments of the magnetic and electric dipoles in the two split rings at resonance. The solid and dashed arrows represent magnetic and electric dipole moments, respectively. Reprinted from Ref. [36].

Figure 7. a) Schematic representation of the 180°-rotated split-ring pair on a glass substrate. The size of each split ring is 400×400 nm². The arm width is 100 nm and the gold thickness is 50 nm. The separation between the two split rings is 50 nm. The normally incident light is polarized along the *x* direction. b) Simulated transmittance and reflectance spectra of the 180°-rotated split-ring pair. The symbols represent the currents in the split rings at the resonance frequency. c) Schematic diagram of the alignments of the magnetic and electric dipoles in the two split rings at resonance. The solid and dashed arrows represent magnetic and electric dipole moments, respectively. Reprinted from Ref. [36].
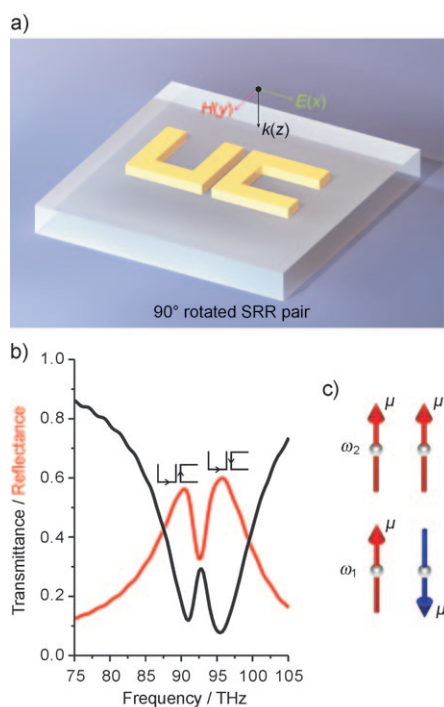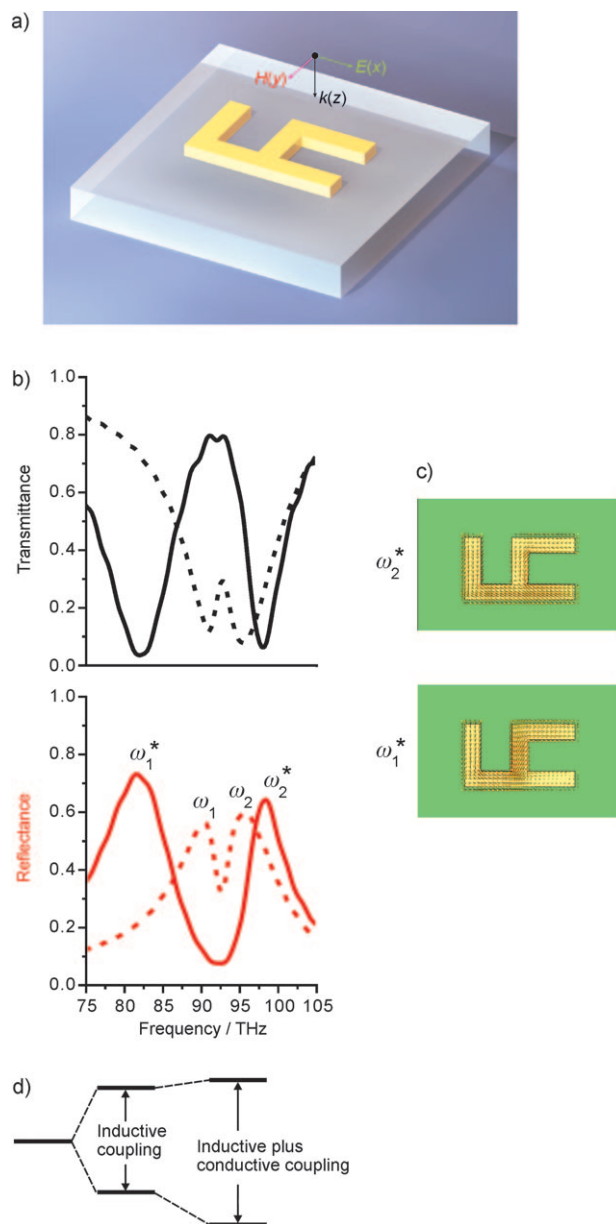
Figure 8. a) Schematic representation of the 90°-rotated split-ring pair on a glass substrate. The size of each split ring is 400×400 nm². The arm width is 100 nm and the gold thickness is 50 nm. The separation between the two split rings is 50 nm. The normally incident light is polarized along the *x* direction. b) Simulated transmittance and reflectance spectra of the 90°-rotated split-ring pair. The symbols represent the currents in the split rings at the resonance frequency. c) Schematic diagram of the alignment of the magnetic dipoles in the two split rings at the respective resonances. The solid arrows represent magnetic dipole moments. Reprinted from Ref. [36].

The electromagnetic coupling strength between the 90°-rotated split-ring pair can be altered by changing their relative distance. The distance between the centers of the two split rings cannot be decreased significantly because of the horizontal side-by-side arrangement. A stronger coupling strength is expected for vertically stacked split rings, which are longitudinally coupled and can be very closely spaced (see Section 5).[38, 65] The two split rings can be physically connected, as illustrated in Figure 9a, to effectively improve the

Figure 9. a) Schematic representation of the connected split-ring pair on a glass substrate. The size of each split ring is 400×400 nm². The arm width is 100 nm and the gold thickness is 50 nm. The normally incident light is polarized along the *x* direction. b) Simulated transmittance and reflectance spectra of the connected split-ring pair. The spectra in Figure 8b are replotted with dashed curves for comparison. c) Current distributions at the respective resonance frequncies. d) Schematic illustration of the asymmetric shift. Reprinted from Ref. [36].

polarization. This introduces phase retardation between the two split rings. The external light couples to the left split ring. At the resonance frequency the mutual inductance between the two elements results in excitation from the left split ring being transferred to the right split ring by inductive coupling.[59–61]

The fact that the electric dipoles excited in the two split rings are perpendicular to each other means that the electric dipole–dipole interaction is zero to a first approximation.[36, 38, 42] As a result, the coupling between the two magnetic dipoles plays a key role and leads to the spectral splitting of the resonance (Figure 8b). In analogy to the states of two simple atoms hybridized into molecular orbitals[48–52] we term the resulting coupled system a "split-ring molecule", in which the two split-ring "atoms" are coupled inductively because of the structural asymmetry.[62–64] The two magnetic dipoles are aligned antiparallel and parallel at the lower and higher resonances, respectively (Figure 8c). This complies with the hybridization picture of two transversely coupled dipoles. In the antisymmetric mode the north and south poles of the two neighboring magnetic dipoles attract each other, and therefore lead to the lower resonance frequency. In the symmetric mode the poles with same sign are repulsive, which leads to the higher resonance frequency.

coupling strength in the planar split-ring pair. This can be termed conductive coupling.[36, 37] The simulated spectra are presented in Figure 9b. For the sake of a direct comparison the spectrum of Figure 8b is replotted as a dashed curve in Figure 9b. The spectral splitting that is directly correlated with the electromagnetic coupling strength is substantially enhanced in the connected structure. In particular, the antisymmetric mode (the lower resonance frequency) shows a red-shift, which is stronger than the blue-shift of the symmetric mode (the higher resonance frequency). Current distributions at corresponding resonances are given in Figure 9c to highlight the underlying physics of the asymmetric shift. In the case of the antisymmetric mode the connecting part acts as a link between two split rings. This allows the currents to contribute positively for both constituents. Consequently, in addition to enhanced inductive coupling because of the reduced distance, conductive coupling from the common conduction currents aids in further increasing the coupling strength between the two split rings. On the other hand, in the case of the symmetric mode, the currents from the connecting part contribute oppositely for both constituents. As a result, the interaction between the two components predominantly remains because of inductive coupling. Hence, the symmetric modes do not show prominent shifts when compared with those of the separated 90°-rotated split rings. A schematic illustration of the asymmetric shift is depicted in Figure 9d.

5. Vertical Coupling of Split-Ring Resonators (Stereo-Metamaterials)

In this section we study a set of *vertically* coupled split-ring dimers. Each dimer has unit cells that consist of two stacked split rings with an identical geometry, but the two split rings are arranged in space with different twist angles. We term these structures *stereo-metamaterials*,[38] in analogy to the concept of stereoisomers in chemistry,[66] where atoms are arranged in molecules with different three-dimensional arrangements. We will show that the optical properties of these stereo-split-ring dimers can be modified substantially by altering the twist angles between the two split-ring "atoms". This arises from the variation in the interactions,[38] particularly how the electric and magnetic interactions depend on the spatial arrangement of these split-ring constituents.

5.1. Spectral Characteristics of Stereo-Metamaterials

We first consider the 0°-twisted split-ring dimer. Two resonances can be observed (ω_0^- and ω_0^+) in the simulated spectrum, as shown in Figure 10a. The normally incident light is polarized along the gap-bearing side of the top split ring. The electric component of the incident light can excite circulating currents along the two split rings, thereby giving rise to induced magnetic dipole moments. As shown in Figure 10b, the electric dipoles excited in the two split rings oscillate anti-phase and in-phase at resonances ω_0^- and ω_0^+, respectively. The resulting magnetic dipoles are aligned
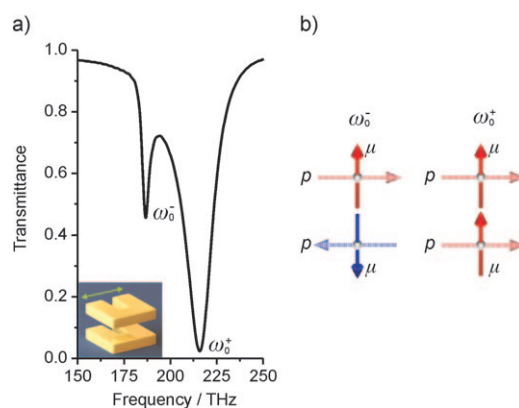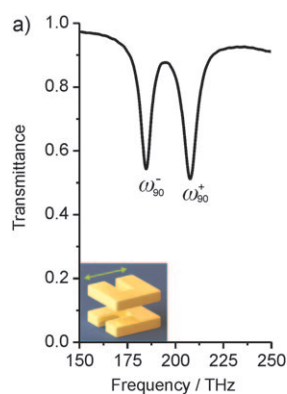

Figure 10. a) Simulated transmittance spectra for the 0°-twisted split-ring dimer metamaterial. The size of each split ring is 230×230 nm². The arm width is 90 nm and the gold thickness is 50 nm. The vertical spacing between the two split rings is 50 nm. The structure is embedded in air. The normally incident light is polarized along the gap-bearing side of the top split ring. b) Schematic diagram of the alignments of the magnetic and electric dipoles in the two split rings at the respective resonance frequencies. The solid and dashed arrows represent the magnetic and electric dipole moments, respectively. Reprinted from Ref. [38], with permission from the Nature Publishing Group.

antiparallel at resonance ω_0^-, whereas they are parallel at resonances ω_0^+.[48–52] In the hybridization model[48–52] the two split-ring "atoms" are bonded into a split-ring dimer or "molecule" because of the strong interaction between them. Such an interaction leads to the formation of new plasmonic modes, which arise from the hybridization of the original state of an individual split-ring mode. The two excited electric dipoles are transversely coupled, while the two magnetic dipoles are longitudinally coupled.

In the case of transverse dipole–dipole interaction the antisymmetric and symmetric modes are at the lower and higher resonance frequencies, respectively. In contrast, in the case of longitudinal dipole–dipole interaction the two magnetic dipoles should align parallel at the lower resonance frequency and antiparallel at the higher resonance frequency. It is evident that for the 0°-twisted stacked split-ring dimer system the resonance levels are determined according to the picture of transverse electric dipole–dipole interaction, with the antisymmetric mode having the lower resonance frequency and the symmetric mode having the higher resonance frequency. In essence, the two coupling mechanisms—the electric and magnetic dipolar interactions—counteract one another and the electric interaction dominates in this system. We will show later that these opposing interactions leads to the splitting of the resonance frequencies not being as large as, for example, in the case of the 180°-twisted arrangement.

For the 90°-twisted split-ring dimer the circular currents in the bottom split ring cannot be excited directly by the incident light because of its orientation with respect to the external electric field. Nevertheless, for the coupled dimer system, at the resonance frequency, excitation from the upper split ring can be transferred to the underlying one by inductive coupling between the two split rings.[38, 65] This leads to the formation of new plasmonic modes (ω_{90}^- and ω_{90}^+), as shown in Figure 11a.

Figure 11. a) Simulated transmittance spectra for the 90°-twisted split-ring dimer metamaterial. The size of each split ring is 230×230 nm^2. The arm width is 90 nm and the gold thickness is 50 nm. The vertical spacing between the two split rings is 50 nm. The structure is embedded in air. The normally incident light is polarized along the gap-bearing side of the top split ring. b) Schematic diagram of the alignment of the magnetic dipoles in the two split rings at the respective resonance frequencies. The solid arrows represent the magnetic dipole moments. Reprinted from Ref. [38], with permission from the Nature Publishing Group.
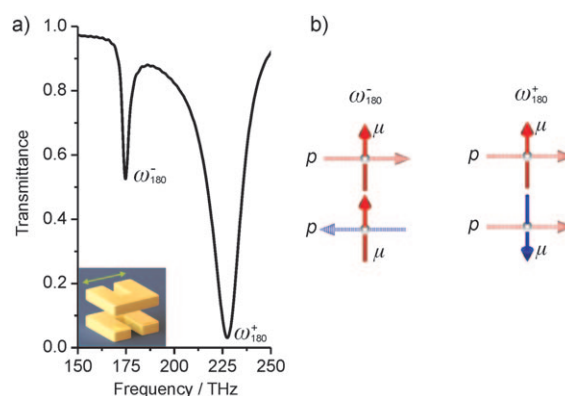
Figure 12. a) Simulated transmittance spectra for the 180°-twisted split-ring dimer metamaterial. The size of each split ring is 230×230 nm^2. The arm width is 90 nm and the gold thickness is 50 nm. The vertical spacing between the two split rings is 50 nm. The structure is embedded in air. The normally incident light is polarized along the gap-bearing side of the top split ring. b) Schematic diagram of the alignments of the magnetic and electric dipoles in the two split rings at the respective resonance frequencies. The solid and dashed arrows represent the magnetic and electric dipole moments, respectively. Reprinted from Ref. [38], with permission from the Nature Publishing Group.

Since the electric fields in the slit gaps of the two split rings are perpendicular to one another, the electric dipole–dipole interaction equals zero. In addition to the fact that the higher-order multipolar interaction is negligible to a first approximation,[36,38,42] the electric coupling in the 90°-twisted split-ring dimer system can thus be ignored. As a consequence, the resonance levels are determined from the longitudinal magnetic dipole–dipole coupling. As shown in Figure 11b, the resulting magnetic dipoles in the two split rings are aligned parallel and antiparallel at resonances ω_{90}^- and ω_{90}^+, respectively.

For the 180°-twisted split-ring dimer, the interaction between the two split rings results in the new plasmonic modes ω_{180}^- and ω_{180}^+ (Figure 12a). As shown in Figure 12b, resonances ω_{180}^- and ω_{180}^+ are associated with the excitation of the electric dipoles in the two split rings oscillating anti-phase and in-phase, respectively. The two resulting magnetic dipoles are thus aligned parallel and antiparallel, respectively. In essence, the transverse electric and longitudinal magnetic interactions contribute positively in the 180°-twisted dimer system. This leads to the largest spectral splitting, which is a direct indication of the coupling strength. It is also worth mentioning that electric coupling plays a key role in 0°- and 180°-twisted split ring dimers. In both cases, the electric dipoles in the two split rings oscillate anti-phase at the lower resonance frequencies (ω_0^- and ω_{180}^-). Such resonances are not easily excited by light, that is, they are subradiant in character.[53] On the other hand, at the higher resonance frequencies (ω_0^+ and ω_{180}^+) the electric dipoles in the two split rings oscillate in-phase. Such resonances can strongly couple to light, that is, they are superradiant in character. As a result, resonances ω_0^- and ω_{180}^- are much less pronounced in width and magnitude with respect to resonances ω_0^+ and ω_{180}^+, respectively (see Figures 10a and 12a).

5.2. Twist Dispersion of Stereo-Metamaterials

To gain further insight into the coupling mechanism we investigate the twist dispersion of the stereo-split-ring dimer system. We vary the twist angle from 0° to 180° in steps of 15° and study the associated resonant behavior. We also show how the electric and magnetic interactions depend on the twist angle of the two split rings.

Figure 13 presents the simulated twisting dispersion curves (in black squares), in which the resonance positions
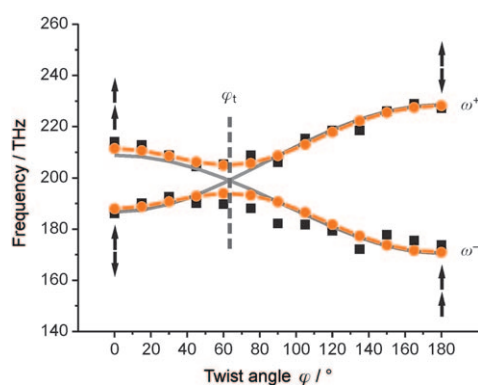
Figure 13. Twisting dispersion of the stereo-split-ring dimer metamaterials. The black squares represent the numerical data. Dashed lines represent the fitting curves calculated from the Lagrangian model with consideration of the higher-order electric multipolar interactions. The avoided crossing is clearly visible at φ_t. The arrows represent the alignment of the magnetic dipoles at lower and higher resonance frequencies at twist angles $\varphi = 0°$ and 180°. The dashed gray lines represent the fitting curves calculated from the Lagrangian model *without* considering the higher-order electric multipolar interactions. No avoided crossing is observable in this case. Reprinted from Ref. [38], with permission from the Nature Publishing Group.

are extracted from the transmittance spectra of different structures. It is apparent that by increasing the twist angle ϕ the two resonance branches first tend to converge, with the ω^+ branch shifting to lower frequencies while the ω^- branch shifts to higher frequencies. An avoided crossing is observed at angle ϕ_t, which is around 60°. The two branches shift away from one another at higher twisting angles. We introduce a Lagrangian formalism to clarify the underlying physics of the twisting dispersion curves.[38,65] One split ring can be modeled by an equivalent inductivity/capacity (LC) circuit with a resonance frequency $\omega_f = 1/(LC)^{-1/2}$.[12] It consists of a magnetic coil (the metal ring) with inductance L and a capacitor (the slit of the ring) with capacitance C. If we define the total charge Q accumulated in the slit as a generalized coordinate, the Lagrangian function of a split ring can be written as $\Gamma = L\dot{Q}^2/2 - Q^2/2C$. Here, $L\dot{Q}^2/2$ refers to the kinetic energy of the oscillations, and $Q^2/2C$ is the electrostatic energy stored in the slit. Consequently, the Lagrangian function of the coupled split-ring dimer systems is a combination of two individual split-ring resonators with the additional electric and magnetic interaction terms shown in Equation (3).

$$\Gamma = \frac{L}{2}\left(\dot{Q}_1^2 - \omega_f^2 Q_1^2\right) + \frac{L}{2}\left(\dot{Q}_2^2 - \omega_f^2 Q_2^2\right) + M_H \dot{Q}_1 \dot{Q}_2$$
$$- M_E \omega_f^2 Q_1 Q_2 \cdot \left(\cos\varphi - \alpha \cdot (\cos\varphi)^2 + \beta \cdot (\cos\varphi)^3\right) \quad (3)$$

Here, Q_1 and Q_2 are oscillating charges in the respective split rings, and M_H and M_E are the mutual inductances for magnetic and electric interactions, respectively. Apart from the electric dipole–dipole interaction, the contributions from the higher-order electric multipolar interactions are also included.[43,44] α and β are the coefficients of the quadrupolar and octupolar plasmon interactions, respectively. They serve as correction terms for the electric dipolar interaction. It is straightforward to derive from Equation (3) that the major interaction items for the 0° and 180° cases are $M_H \dot{Q}_1 \dot{Q}_2 - M_E \omega_f^2 Q_1 Q_2$ and $M_H \dot{Q}_1 \dot{Q}_2 + M_E \omega_f^2 Q_1 Q_2$, respectively. The finding that the magnetic and electric interactions contribute oppositely and positively in the 0°- and 180°-twisted cases, respectively, is in accord with the above simulation results. For the 90°-twisted split-ring dimer, only the magnetic interaction plays a key role, as represented by the interaction term $M_H \dot{Q}_1 \dot{Q}_2$. Subsequently, by solving the Euler–Lagrange Equations (4), the eigenfrequencies of these stereo-split-ring dimer systems can be obtained from Equation (5), where $\kappa_E = M_E/L$ and $\kappa_H = M_H/L$ are the coefficients of the overall electric and magnetic interactions, respectively.

$$M_H \dot{Q}_1 \dot{Q}_2 \frac{d}{dt}\left(\frac{\partial \Gamma}{\partial \dot{Q}_i}\right) - \frac{\partial \Gamma}{\partial Q_i} = 0, \quad (i = 1, 2) \quad (4)$$

$$\omega_\pm = \omega_0 \cdot \sqrt{\frac{1 \mp \kappa_E \cdot \left(\cos\varphi - \alpha \cdot (\cos\varphi)^2 + \beta \cdot (\cos\varphi)^3\right)}{1 \mp \kappa_H}} \quad (5)$$

Fitting the twisting dispersion curves leads to the corresponding coefficients being estimated as $\kappa_E = 0.14$, $\kappa_H = 0.09$, $\alpha = 0.8$, and $\beta = -0.4$. It is notable that the fitted curves (dashed lines in Figure 13) reproduce the numerical data

quite well and the avoided crossing is clearly observable at around 60°. This finding shows that the Lagrangian model can corroborate the results from the numerical simulations quantitatively. It is of crucial importance that the higher-order electric multipolar interactions account for the existence of the avoided crossing. The finite length of the split ring means that discrete electric plasmon modes characterized by different spatial symmetries can be excited by the incident light.[67,68] The gray solid lines in Figure 13 display the twisting dispersion curves in which only the dipolar coupling effect is taken into account, namely, $\alpha = 0$ and $\beta = 0$, and hence highlight the significant role of the higher-order electric multipolar interactions. The best fit is achieved with $\kappa_E = 0.2$ and $\kappa_H = 0.09$. Although the gray curves can fit most parts of the numerical data, no avoided crossing is predicted. Instead, the ω^+ and ω^- branches converge at ϕ_t.

Therefore, it must be emphasized that although the electric and magnetic dipolar interactions are the essential mechanisms, the higher-order electric multipolar interactions should also be considered carefully to fully understand the origin of the spectral characteristics of the stereo-metamaterial systems.

6. Three-Dimensional Metamaterials

6.1. Stacked Nanowire Metamaterials

Let us turn in this section to more complex metamaterials. First, we investigate a four-layer stacked nanowire metamaterial.[40] Figure 14a shows the simulated transmittance spectrum, where four resonances are observed at different frequencies. In fact, it is more straightforward to understand the resonant behavior by regarding the system as two coupled nanowire pairs.[40,48] A single coupled nanowire pair can lead to a symmetric mode and an antisymmetric mode. As shown in Figure 14b, the ω_+^+ and ω_-^- modes actually result from the interaction of the symmetric modes of the two nanowire pairs.
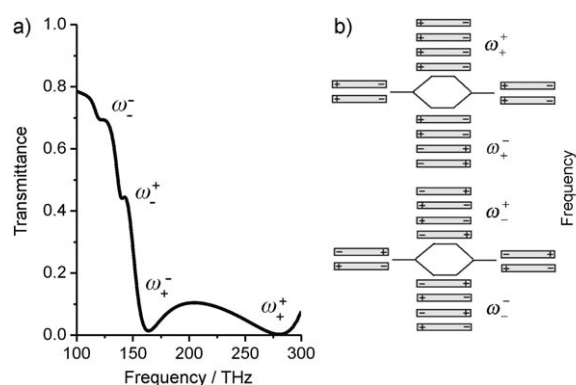

Figure 14. Simulated transmittance spectrum for four coupled nanowires. The size of the individual nanowires is $500 \times 150 \times 20$ nm³. The vertical spacing between nanowires is 80 nm. The light is incident along the stacking direction, with a linear polarization along the longer axis of the nanowires. b) Schematic illustration of the resonance diagram depicting the hybridization of the modes for the stacked nanowire structure. Reprinted from Ref. [40].

In the case of the ω_+^+ mode the charge oscillations inside the four wires are all in-phase, and thus the restoring forces between neighboring nanowires are all repulsive. This leads to the ω_+^+ mode having the highest resonant frequency among the four modes. Similar to the antisymmetric mode in the case of two coupled nanowires, the ω_+^- mode can be interpreted in terms of a magnetic resonance. Simultaneously, the generation of the ω_-^- and ω_-^+ modes results from the coupling of the antisymmetric modes of the two nanowire pairs. The ω_-^- mode has the lowest resonance frequency because the charge oscillation inside each nanowire in this case is out of phase with respect to its neighboring wire(s), and therefore the restoring forces between neighboring wires are all attractive. Similarly, the ω_-^- and ω_+^- modes, which would be dark at the quasistatic limit, can be excited by light in a real system as a consequence of phase retardation. In principle, a coupling also exists between the symmetric and antisymmetric modes of the two nanowire pairs, but it can be ignored due to the larger frequency separation (and thus lower coupling intensity).[48]

6.2. Stacked Split-Ring Resonator Metamaterials

In this section we discuss the optical properties of a four-layer stacked split ring metamaterial[32,42] with its individual constituents twisted by 90° with respect to their neighbors (Figure 15). We excite this metamaterial structure with linearly polarized light along the gap-bearing side of the top split ring at normal incidence and record its transmission spectrum. Four resonances are observed, as shown in Figure 16a. These resonances bear evidence of the modes that arise as a result of coupling between the four split rings. We will examine these resonances according to our previously introduced coupling principles. First, we notice that the next-neighbor electrical dipole–dipole interaction is zero to a first approximation, as the electrical dipoles are perpendicular to each other.[36,38,42] Hence, we are left with the magnetic dipole–dipole interaction between the adjacent split rings. In this case, we encounter a longitudinal coupling.
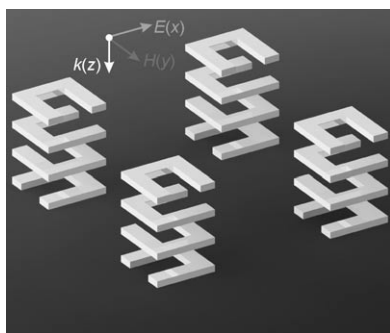

Figure 15. Geometry of a four-layer twisted split-ring metamaterial. The size of each split ring is 400×400 nm^2. The arm width is 100 nm and the gold thickness is 60 nm. The vertical spacing between the adjacent split rings is 60 nm. The normally incident light is polarized along the gap-bearing side of the top split ring. Reprinted from Ref. [42], with permission from the Optical Society of America.
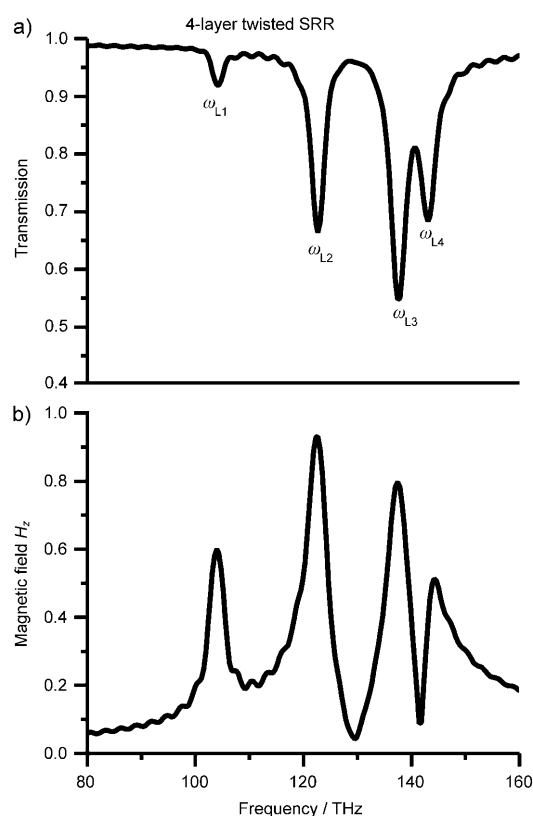
Figure 16. a) Simulated transmission spectrum (L1–L4 = longitudinally coupled split rings) and b) field strength of the H_z component of the four-layer twisted split-ring metamaterial. The probe for the H_z component is positioned at the center of the uppermost split ring. Reprinted from Ref. [42] with permission from the Optical Society of America.

As the examination of the z components of the magnetic fields shows (Figure 16b), the lowest frequency resonance is the one where all the magnetic dipoles are aligned in parallel, as we would expect for longitudinal coupling (Figure 17). In analogy to solid-state physics, one might call this state a "ferromagnetic" one.[34] As we deal with optical frequencies, one might even interpret this ground state as "optical ferromagnetism". However, we need to be careful with this nomenclature. As solid-state physicists point out, ferromagnetism is a quantum phenomenon that is mediated by the spin-exchange interaction.[34] For spins we have a Pauli exclusion principle. Also, ferromagnetism exhibits a hysteresis, which is associated with a phase transition, and still remains in place after the magnetic field is turned off. However, in our case, we have purely classical fields ("classical spins") with no Pauli exclusion principle. In addition, no magnetic field is left in the split rings a few femtoseconds after the light field has been turned off because of the radiative and nonradiative damping. Therefore, this parallel alignment of the magnetic moments in the ground state might be better termed "optical superparamagnetism", which is closer to its solid-state physics counterpart.[39,61]

The higher frequency modes show alignment of their magnetic dipole moments, similar to the principles that we use when considering wavefunctions in a harmonic oscillator
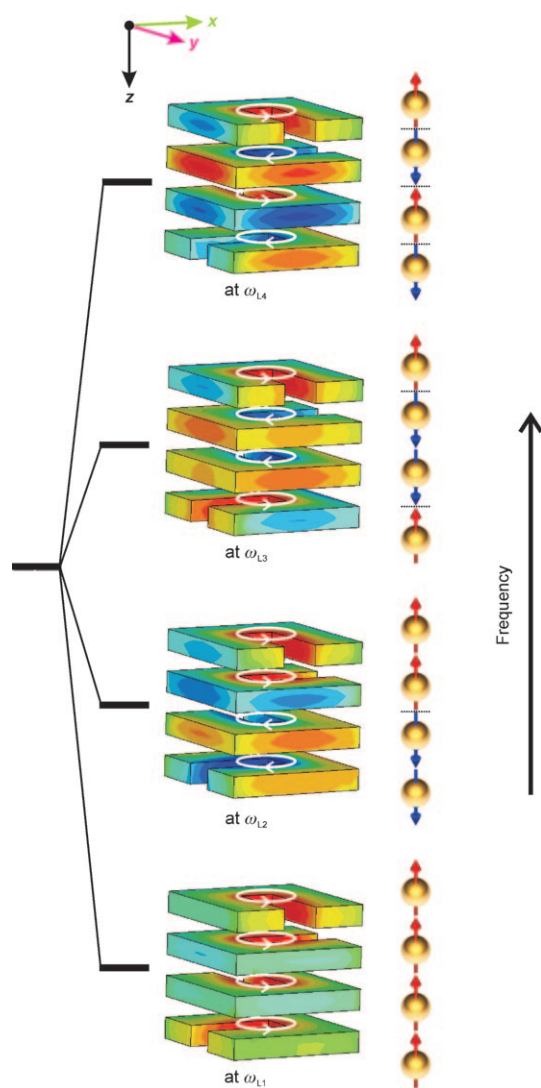
Figure 17. Resonance diagram depicting the hybridization of the modes for the four-layer twisted split-ring metamaterial and the simulated magnetic field distributions of H_z at the corresponding resonance frequencies. The light is incident along the z direction and linearly polarized along the x direction. Red denotes a positive H field, and blue denotes a negative H field. The "spin" symbols (right) represent the magnetic dipole moments for the respective modes. The number of magnetic field nodes (dotted lines) rises with increasing resonance frequencies. Reprinted from Ref. [42], with permission from the Optical Society of America.

potential.[69] In this case, one can simply count the number of nodes in such a potential, starting at zero nodes for the ground state and increasing the number of nodes in the wavefunction for each higher-order state. Specifically, we find that our total "classical spin" wavefunction of the stacked split-ring system has zero nodes (namely, flips in the neighboring magnetic moments) for the lowest frequency resonance. The number of nodes then increases to one, two, and three for the higher frequency modes. The highest frequency resonance has three nodes, which renders the entire "spin system" totally anti-parallel. An illustration of the alignment of magnetic dipole

moments at different resonance frequencies is shown in Figure 17.

6.3. Stacked Fishnet Metamaterials

Transverse coupling between magnetic dipoles can be realized in a three-dimensional stacked fishnet metamaterial through side-by-side arrangement.[41, 42, 70–72] As shown in Figure 18, the fishnet layers of gold are surrounded by air, and the wire widths in both directions are designed to be equal for polarization independence.
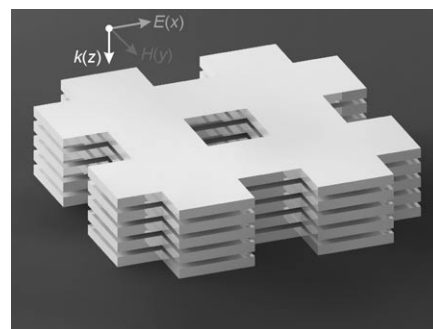

Figure 18. Geometry of a five-layer fishnet metamaterial. The width of each wire is 350 nm. The thickness of the gold is 40 nm and the vertical spacing between wires is 20 nm. The normally incident light is polarized along the x direction. Reprinted from Ref. [42], with permission from Optical Society of America.

The simulated transmission spectrum is presented in Figure 19a, in which four resonances are clearly evident. Additionally, a large enhancement of the localized magnetic field at the corresponding resonance frequencies is observed by detecting the amplitudes of the magnetic field H_y with a probe placed inside the gap between the top two gold wires. (Figure 19b) Each resonance is associated with the excitation of magnetic dipole moments inside the four gaps between each pair of gold wires.

The resonant behavior of the stacked fishnet system can also be understood with the help of the hybridization of the magnetic response. The incident light excites a current loop in each wire pair, which results in a magnetic dipole moment.[13, 14, 70–74] These magnetic dipoles are transversely coupled, thereby leading to the formation of four new hybridized modes, which are associated with different symmetries. More specifically, the four magnetic dipoles align fully antiparallel at the lowest frequency resonance. The intermediate resonances correspond to incomplete antiparallel arrangements of the magnetic dipoles, whereas at the highest resonance frequency the four magnetic dipoles are aligned fully parallel. Figure 20 shows the interaction between these transversely coupled magnetic dipoles and the resulting hybridized modes.

Intuitively, a spectral band consisting of different frequency levels will be formed when more and more such metamaterial elements are included,[41] just like the case in solid-state physics. The bandwidth is given by the original

© 2010 Wiley-VCH Verlag GmbH & Co. KGaA, Weinheim
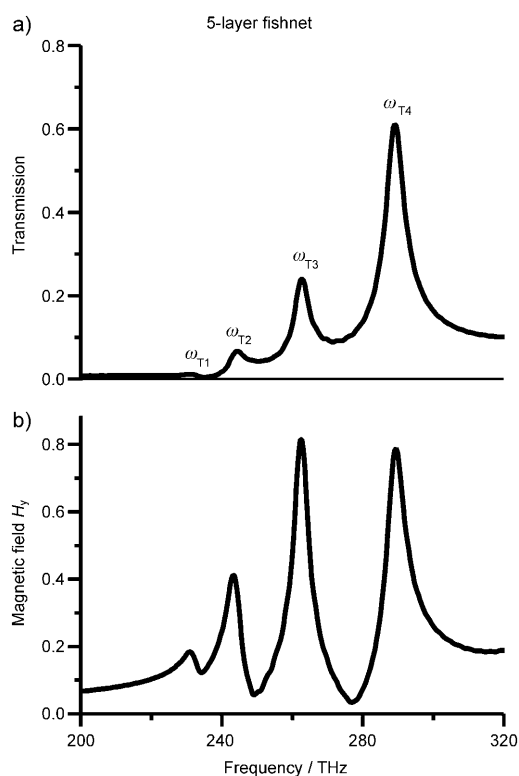
Figure 19. a) Simulated transmission spectrum and b) detected H_y intensities for the five-layer fishnet metamaterial. The H_y probe is positioned inside the gap between the top two gold wires. Reprinted from Ref. [42], with permission from the Optical Society of America.

coupling strength of two nearest neighbors, which is similar to a tight binding model.[34] The schematic diagram shown in Figure 21 illustrates the formation of the resonance band.

6.4. Complex Three-dimensional Metamaterials

We are now going to combine the concepts of longitudinal and transverse coupling to arrange metamaterial magnetic dipoles in three dimensions.[42] In our design, the combination of longitudinal and transverse coupling is unique in the sense that it allows for the study of purely magnetic dipole–dipole interactions in a metasolid in the lateral as well as in the vertical direction (as far as solely nearest neighbor interactions are considered). Figure 22 a shows a planar unit cell of such an element, which consists of four split rings at an angle of 90° relative to their neighbors. Longitudinal coupling can be introduced as a complication to the two-dimensional prototype by subsequently stacking the planar building blocks, with each layer twisted by 90° compared to its former layer. The coupling strengths of the longitudinal as well as the transverse coupling can be controlled by altering the lateral and vertical separations of the constituent split rings. Figure 22 b illustrates the three-dimensional arrangement of these split rings, which constitutes a magnetic metasolid. We might term it a "photonic spin crystal". The future challenge lies in understanding the rather complicated spectra of such magnetic systems and examining their
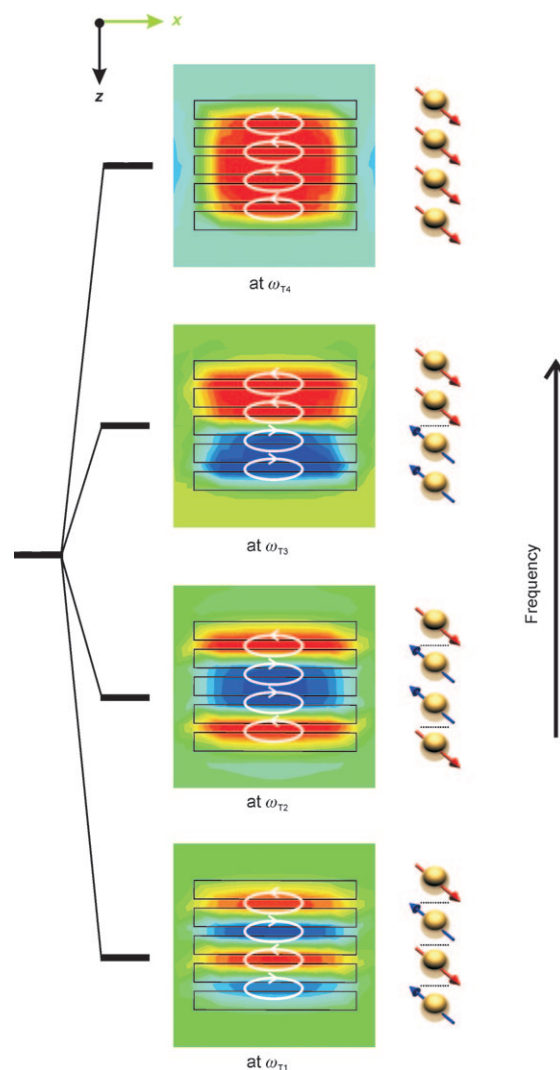

Figure 20. Resonance diagram depicting the hybridization of the modes for the five-layer fishnet metamaterial and the simulated magnetic field distributions of H_y at the corresponding resonance frequencies. The light is incident along the z direction and linearly polarized along the x direction. Red denotes a positive H field, and blue denotes a negative H field. The "spin" symbols (right) represent the magnetic dipole moments for the respective modes. The number of magnetic field nodes (dotted lines) declines with increasing resonance frequencies. Reprinted from Ref. [42], with permission from the Optical Society of America.

collective modes, which are analogous to spin waves and magnons in solid-state physics.[34]

7. Summary and Outlook

In this Review we demonstrated how coupling plays a dominant role in the optical properties of metamaterials. Starting from plasmon hybridization, a concept that is borrowed from molecular physics, we explained how bringing two plasmonic nanoparticles into proximity result in their coupling together and the formation of hybridized modes. We then discussed how the coupling and symmetry rules were
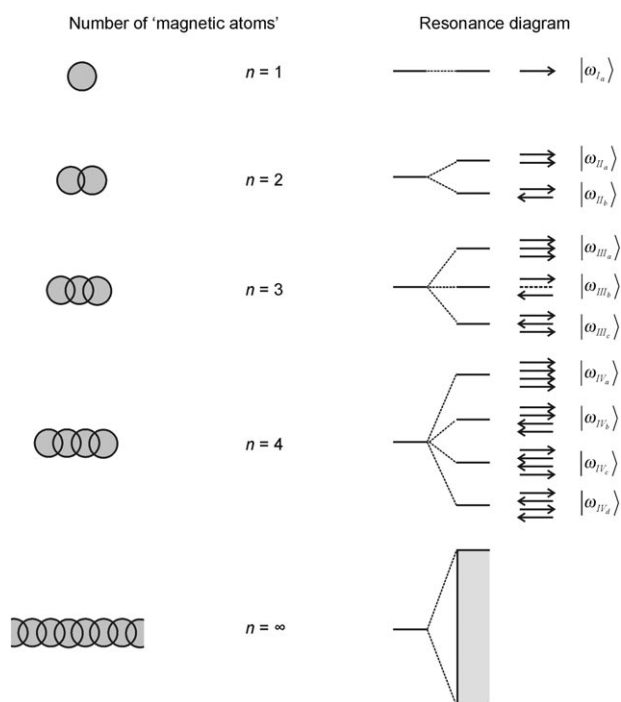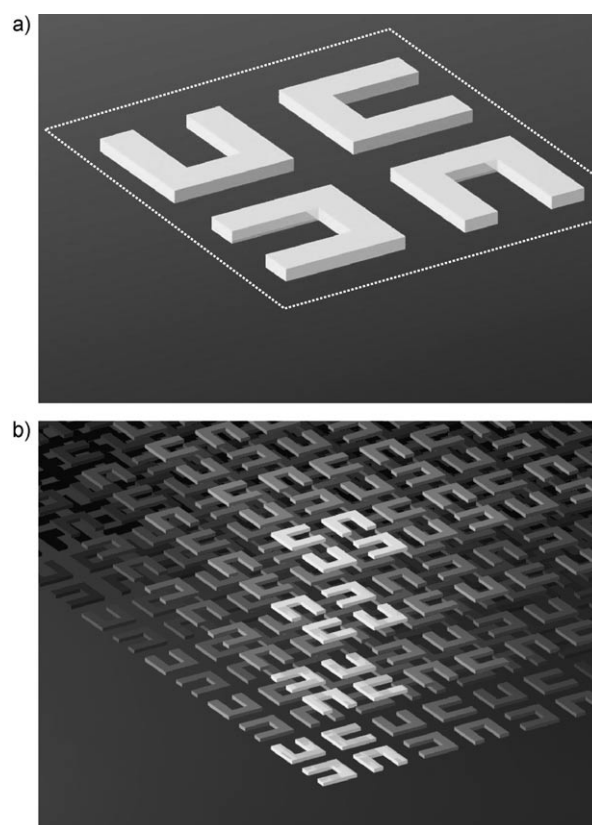
Figure 21. The formation of the resonance band arising from the coupling between magnetic "atoms". Two "atoms" form "molecular" states by hybridization, which emerge into bands when many "atoms" are coupled. Reprinted from Ref. [41].

Figure 22. a) A unit cell of a two-dimensional magnetic metamaterial. b) A hypothetical three-dimensional magnetic ("spin") metamaterial. Each layer consists of split rings that are twisted by 90° compared to its vertical neighbor layers. Reprinted from Ref. [42], with permission from the Optical Society of America.

dependent on the coupling geometry and on the incoming polarization of the light.

This concept was extended to split rings, which are basic constituents of metamaterials and exhibit, in addition to the electric dipole moment, a magnetic dipole moment at optical frequencies. Both electric as well as magnetic coupling occurs when such split-ring resonators are coupled together. Either one can dominate, depending on the exact structural geometry. In the special case of 90°-twisted split rings, to a first approximation, the electric dipole–dipole interaction is turned off and magnetic dipole–dipole interaction dominates.

We also applied the well-known concept of stereochemistry to our stereo-metamaterials. These are metamaterials with the same constituents but which are arranged in different spatial configurations. We found that the twisting dispersion is crucial for understanding the optical properties of such complex metamaterials. In fact, the electric and magnetic coupling can either act against each other or act in concert with each other. Interestingly, an anticrossing in this twisting dispersion occurs, which is direct proof for the existence of higher-order electric multipolar interactions. The tunability of the resonant behavior of metamaterials by altering the spatial arrangement of their constituents offers great flexibility for exploring useful metamaterial properties, such as chirality[75–79] and optical activity.[80–82]

We also considered several three-dimensional metamaterial structures and extended our coupling rules to a larger number of metamaterial "atoms". Adding more and more coupled constituents can lead to the formation of spectral bands. Taking a step further, one might even consider the coupling between dipoles and higher-order multipoles in metamaterials.[83–85] For example, stacking a single gold wire above a gold wire pair can enable dipole–quadrupole coupling and lead to a classical analogue of electromagnetically induced transparency.[84–90] This phenomenon allows for very sharp and deep resonances within the plasmonic spectrum and could be utilized for localized surface plasmon resonance sensors in the future.[85,91,92]

[1] D. R. Smith, J. B. Pendry, M. C. K. Wiltshire, *Science* **2004**, *305*, 788–792.
[2] C. M. Soukoulis, S. Linden, M. Wegener, *Science* **2007**, *315*, 47–49.
[3] C. M. Soukoulis, M. Kafesaki, E. N. Economou, *Adv. Mater.* **2006**, *18*, 1941–1952.
[4] V. M. Shalaev, *Nat. Photonics* **2007**, *1*, 41–48.

[5] U. Kreibig, M. Vollmer in *Optical properties of metal clusters*, Springer, Berlin, **1995**.

[6] C. F. Bohren, D. R. Hufman in *Absorption and scattering of light by small particles*, Wiley-VCH, New York, **1983**.

[7] U. Kreibig, P. Zacharias, *Z. Phys.* **1970**, *231*, 128–143.

[8] M. C. Daniel, D. Astruc, *Chem. Rev.* **2004**, *104*, 293–346.

[9] V. A. Podolskiy, A. K. Sarychev, V. M. Shalaev, *Opt. Express* **2003**, *11*, 735–745.

[10] V. A. Podolskiy, A. K. Sarychev, E. E. Narimanov, V. M. Shalaev, *J. Opt. A* **2005**, *7*, S32–S37.

[11] J. B. Pendry, A. J. Holden, D. J. Robbins, W. J. Stewart, *IEEE Trans. Microwave Theory Tech.* **1999**, *47*, 2075–2084.

[12] S. Linden, C. Enrich, M. Wegener, J. F. Zhou, T. Koschny, C. M. Soukoulis, *Science* **2004**, *306*, 1351–1353.

[13] S. Zhang, W. J. Fan, K. J. Malloy, S. R. J. Brueck, N. C. Panoiu, R. M. Osgood, *Opt. Express* **2005**, *13*, 4922–4930.

[14] G. Dolling, C. Enrich, M. Wegener, C. M. Soukoulis, S. Linden, *Science* **2006**, *312*, 892–894.

[15] M. S. Rill, C. Plet, M. Thiel, I. Staude, G. von Freymann, S. Linden, M. Wegener, *Nat. Mater.* **2008**, *7*, 543–546.

[16] H. Schweizer, L. Fu, H. Gräbeldinger, H. Guo, N. Liu, S. Kaiser, H. Giessen, *Phys. Status Solidi A* **2007**, *204*, 3886–3900.

[17] G. Dolling, C. Enrich, M. Wegener, J. F. Zhou, C. M. Soukoulis, S. Linden, *Opt. Lett.* **2005**, *30*, 3198–3200.

[18] J. B. Pendry, A. J. Holden, W. J. Stewart, I. Youngs, *Phys. Rev. Lett.* **1996**, *76*, 4773–4776.

[19] V. G. Veselago, *Sov. Phys. Usp.* **1968**, *10*, 509–514.

[20] D. R. Smith, W. J. Padilla, D. C. Vier, S. C. Nemat-Nasser, S. Schultz, *Phys. Rev. Lett.* **2000**, *84*, 4184–4187.

[21] R. A. Shelby, D. R. Smith, S. Schultz, *Science* **2001**, *292*, 77–79.

[22] N. Katsarakis, T. Koschny, M. Kafesaki, E. N. Economou, E. Ozbay, C. M. Soukoulis, *Phys. Rev. B* **2004**, *70*, 201101.

[23] J. F. Zhou, L. Zhang, G. Tuttle, T. Koschny, C. M. Soukoulis, *Phys. Rev. B* **2006**, *73*, 041101.

[24] J. B. Pendry, *Phys. Rev. Lett.* **2000**, *85*, 3966–3969.

[25] N. Fang, H. Lee, C. Sun, X. Zhang, *Science* **2005**, *308*, 534–537.

[26] Z. W. Liu, H. Lee, Y. Xiong, C. Sun, X. Zhang, *Science* **2007**, *315*, 1686.

[27] J. B. Pendry, D. Schurig, D. R. Smith, *Science* **2006**, *312*, 1780–1782.

[28]

D. Schurig, J. J. Mock, B. J. Justice, S. A. Cummer, J. B. Pendry, A. F. Starr, D. R. Smith, *Science* **2006**, *314*, 977–980.

[29] J. Valentine, J. Li, T. Zentgraf, G. Bartal, X. Zhang, *Nat. Mater.* **2009**, *8*, 568–571.

[30] N. Liu, H. Guo, L. Fu, H. Schweizer, S. Kaiser, Harald Giessen, *Phys. Status Solidi B* **2007**, *244*, 1251–1255.

[31] C. Rockstuhl, T. Zentgraf, H. Guo, N. Liu, C. Etrich, I. Loa, K. Syassen, J. Kuhl, F. Lederer, H. Giessen, *Appl. Phys. B* **2006**, *84*, 219–227.

[32] N. Liu, H. C. Guo, L. W. Fu, S. Kaiser, H. Schweizer, H. Giessen, *Nat. Mater.* **2008**, *7*, 31–37.

[33] J. F. Zhou, T. Koschny, M. Kafesaki, C. M. Soukoulis, *Phys. Rev. B* **2009**, *80*, 035109.

[34] N. W. Ashcroft, N. D. Mermin in *Solid State Physics*, Brooks/Coole Thomson Learning, Singapore, **2003**.

[35] J. D. Jackson in *Classical Electrodynamics*, Wiley-VCH, New York, **1975**.

[36] N. Liu, S. Kaiser, H. Giessen, *Adv. Mater.* **2008**, *20*, 4521–4525.

[37] H. Liu, D. A. Genov, D. M. Wu, Y. M. Liu, J. M. Steele, C. Sun, S. N. Zhu, X. Zhang, *Phys. Rev. Lett.* **2006**, *97*, 243902.

[38] N. Liu, H. Liu, S. Zhu, H. Giessen, *Nat. Photonics* **2009**, *3*, 157–162.

[39] M. Decker, S. Linden, M. Wegener, *Opt. Lett.* **2009**, *34*, 1579–1581.

[40] N. Liu, H. C. Guo, L. W. Fu, S. Kaiser, H. Schweizer, H. Giessen, *Adv. Mater.* **2007**, *19*, 3628–3632.

[41] N. Liu, L. W. Fu, S. Kaiser, H. Schweizer, H. Giessen, *Adv. Mater.* **2008**, *20*, 3859–3865.

[42] N. Liu, H. Giessen, *Opt. Express* **2008**, *16*, 21233–21238.

[43] J. Petschulat, C. Menzel, A. Chipouline, C. Rockstuhl, A. Tünnermann, F. Lederer, T. Pertsch, *Phys. Rev. A* **2008**, *78*, 043811.

[44] D. J. Cho, F. Wang, X. Zhang, Y. R. Shen, *Phys. Rev. B* **2008**, *78*, 121101.

[45]

W. S. Cai, U. K. Chettiar, H. K. Yuan, V. C. de Silva, A. V. Kildishev, V. P. Drachev, V. M. Shalaev, *Opt. Express* **2007**, *15*, 3333–3341.

[46] G. Shvets, Y. A. Urzhumov, *J. Opt. A* **2006**, *8*, S122–S130.

[47] H. K. Yuan, U. K. Chettiar, W. S. Cai, A. V. Kildishev, A. Boltasseva, V. P. Drachev, V. M. Shalaev, *Opt. Express* **2007**, *15*, 1076–1083.

[48] E. Prodan, C. Radloff, N. J. Halas, P. Nordlander, *Science* **2003**, *302*, 419–422.

[49] H. Wang, D. W. Brandl, F. Le, P. Nordlander, N. J. Halas, *Nano Lett.* **2006**, *6*, 827–832.

[50] F. Hao, C. L. Nehl, J. H. Hafner, P. Nordlander, *Nano Lett.* **2007**, *7*, 729–732.

[51] P. Nordlander, C. Oubre, E. Prodan, K. Li, M. I. Stockman, *Nano Lett.* **2004**, *4*, 899–903.

[52] J. B. Lassiter, J. Aizpurua, L. I. Hernandez, D. W. Brandl, I. Romero, S. Lal, J. H. Hafner, P. Nordlander, N. J. Halas, *Nano Lett.* **2008**, *8*, 1212–1218.

[53] A. Christ, T. Zentgraf, S. G. Tikodeev, N. A. Gippius, J. Kuhl. H. Giessen, *Phys. Rev. B* **2006**, *74*, 155435.

[54] P. K. Jain, S. Eustis, M. A. El-Sayed, *J. Phys. Chem. B* **2006**, *110*, 18243–18253.

[55] M. Gluodenis, C. A. Foss, Jr., *J. Phys. Chem. B* **2002**, *106*, 9484–9489.

[56] C. Enrich, F. P-Willard, D. Gerthsen, J. F. Zhou, T. Koschny, C. M. Soukoulis, M. Wegener, S. Linden, *Adv. Mater.* **2005**, *17*, 2547–2549.

[57] C. Enrich, M. Wegener, S. Linden, S. Burger, L. Zschiedrich, F. Schmidt, J. F. Zhou, T. Koschny, C. M. Soukoulis, *Phys. Rev. Lett.* **2005**, *95*, 203901.

[58] R. Singh, C. Rockstuhl, F. Lederer, W. Zhang, *Phys. Rev. B* **2009**, *79*, 085111.

[59] E. Shamonina, V. A. Kalinin, K. H. Ringhofer, L. Solymar, *J. Appl. Phys.* **2002**, *92*, 6252–6261.

[60] E. Shamonina, L. Solymar, *J. Phys. D* **2004**, *37*, 362–367.

[61] G. Dolling, M. Wegener, A. Schaedle, S. Burger, S. Linden, *Appl. Phys. Lett.* **2006**, *89*, 231118.

[62] F. Hao, P. Nordlander, M. T. Burnett, S. A. Maier, *Phys. Rev. B* **2007**, *76*, 245417.

[63] A. Christ, O. J. F. Martin, Y. Ekinci, N. A. Gippius, S. G. Tikhodeev, *Nano Lett.* **2008**, *8*, 2171–2175.

[64] V. A. Fedotov, M. Rose, S. L. Prosvirnin, N. Papasimakis, N. I. Zheludev, *Phys. Rev. Lett.* **2007**, *99*, 147401.

[65] H. Liu, D. A. Genov, D. M. Wu, Y. M. Liu, Z. W. Liu, C. Sun, S. N. Zhu, X. Zhang, *Phys. Rev. B* **2007**, *76*, 073101.

[66] M. J. T. Robinson in *Organic Stereochemistry*, Oxford University Press, Oxford, **2000**.

[67] C. Rockstuhl, F. Lederer, C. Etrich, T. Zentgraf, J. Kuhl, H. Giessen, *Opt. Express* **2006**, *14*, 8827–8836.

[68] F. Hao, E. M. Larsson, T. A. Ali, D. S. Sutherland, P. Nordlander, *Chem. Rev. Lett.* **2008**, *458*, 262–266.

[69] P. Atkins, R. Friedman in *Molecular Quantum Mechanics*, Oxford University Press, Oxford, **2005**.

[70] J. Valentine, S. Zhang, T. Zentgraf, E. Ulin-Avila, D. A. Genov, G. Bartal, X. Zhang, *Nature* **2008**, *455*, 376–379.

[71] S. Zhang, W. J. Fan, N. C. Panoiu, K. J. Malloy, R. M. Osgood, S. R. J. Brueck, *Opt. Express* **2006**, *14*, 6778–6787.

[72] G. Dolling, M. Wegener, S. Linden, *Opt. Lett.* **2007**, *32*, 551–553.

[73] G. Dolling, C. Enrich, M. Wegener, C. M. Soukoulis, S. Linden, *Opt. Lett.* **2006**, *31*, 1800–1802.

[74] G. Dolling, M. Wegener, C. M. Soukoulis, S. Linden, *Opt. Lett.* **2007**, *32*, 53–55.

[75] J. B. Pendry, *Science* **2004**, *306*, 1353–1355.

[76] A. V. Rogacheva, V. A. Fedotov, A. S. Schwanecke, N. I. Zheludev, *Phys. Rev. Lett.* **2006**, *97*, 177401.

[77] J. K. Gansel, M. Thiel, M. S. Rill, M. Decker, K. Bade, V. Saile, G. Freymann, S. Linden, M. Wegener, *Science* **2009**, *325*, 1513–1515.

[78] M. Thiel, M. S. Rill, G. von Freymann, M. Wegener, *Adv. Mater.* **2009**, *21*, 4680.

[79] S. Zhang, Y. Park, J. Li, X. Lu, W. L. Zhang, X. Zhang, *Phys. Rev. Lett.* **2009**, *102*, 023901.

[80] E. Plum, X.-X. Liu, V. A. Fedotov, Y. Chen, D. P. Tsai, N. I. Zheludev, *Phys. Rev. Lett.* **2009**, *102*, 113902.

[81] E. Plum, V. A. Fedotov, N. I. Zheludev, *Appl. Phys. Lett.* **2008**, *93*, 191911.

[82] M. Decker, M. Ruther, C. E. Kriegler, J. Zhou, C. M. Soukoulis, S. Linden, M. Wegener, *Opt. Lett.* **2009**, *34*, 2501–2503.

[83] N. Verellen, Y. Sonnefraud, H. Sobhani, F. Hao, V. V. Moshchalkov, P. V. Dorpe, P. Nordlander, S. A. Maier, *Nano Lett.* **2009**, *9*, 1663–1667.

[84] N. Liu, L. Langguth, T. Weiss, J. Kästel, M. Fleischhauer, T. Pfau, H. Giessen, *Nat. Mater.* **2009**, *8*, 758–762.

[85] N. Liu, T. Weiss, M. Mesch, L. Langguth, U. Eigenthaler, M. Hirschner, C. Sönnichsen, H. Giessen, *Nano Lett.* **2009**, *10*, 1103.

[86] C. L. Garrido Alzar, M. A. G. Martinez, P. Nussenzveig, *Am. J. Phys.* **2002**, *70*, 37–41.

[87] M. Fleischhauer, A. Imamoglu, J. P. Marangos, *Rev. Mod. Phys.* **2005**, *77*, 633–673.

[88] S. Zhang, D. Genov, Y. Wang, M. Liu, X. Zhang, *Phys. Rev. Lett.* **2008**, *101*, 047401.

[89] P. Tassin, L. Zhang, T. Koschny, E. N. Economou, C. M. Soukoulis, *Phys. Rev. Lett.* **2009**, *102*, 053901.

[90] N. Papasimakis, V. A. Fedotov, N. I. Zheludev, *Phys. Rev. Lett.* **2008**, *101*, 253903.

[91] S. Lal, S. Link, N. J. Halas, *Nat. Photonics* **2007**, *1*, 641–648.

[92] F. Hao, Y. Sonnefraud, P. V. Dorpe, S. A. Maier, N. J. Halas, P. Nordlander, *Nano Lett.* **2008**, *8*, 3983–3988.

9852   **www.angewandte.org**

© 2010 Wiley-VCH Verlag GmbH & Co. KGaA, Weinheim

Angew. Chem. Int. Ed. **2010**, *49*, 9838–9852